Journal of Organometallic Chemistry, 478 (1994) 1–8

Bonding analysis of electron-rich bridged mixed main-group/transition metal tetrahedral M_2E_2 organometallic clusters

Samia Kahlal, Jean-François Halet and Jean-Yves Saillard

Laboratoire de Chimie du Solide et Inorganique Moléculaire, URA CNRS 1495, Université de Rennes I, 35042 Rennes Cedex (France)

Kenton H. Whitmire

Department of Chemistry, Rice University, Houston, TX 77251 (USA)

(Received July 7, 1993)

Abstract

The nature of the E–E interaction in the electron-rich seven skeletal electron-pair mixed main-group/transition metal tetrahedral M_2E_2 organometallic clusters of which the E_2 linkage is spanned by an ML_n fragment, is analyzed with the aid of molecular orbital calculations of extended Hückel-type. The results show that the extra skeletal electron pair is housed in a non-bonding molecular orbital of b_1 symmetry which is the HOMO of the systems. The nature and the peculiar position of this orbital are mainly due to two parameters: the pinch effect of the ML_n bridging unit and the electronegativity difference between the metal and main-group atoms.

Key words: Iron; Cobalt; Bismuth; Selenium; Tellurium; Cluster; Extended Huckel calculations

1. Introduction

The rationalization of the structure and bonding of clusters can be generally achieved within the framework of simple electron counting schemes [1–4], the more convenient of which being probably the so-called polyhedral skeletal electron pair theory (PSEPT) [1,2], which is widely used in organometallic cluster chemistry. However, exceptions to these rules can occur when systems become complicated. Among these exceptions, there are several examples of mixed main-group/transition metal clusters which are considered as being too electron-rich with respect to the structure they adopt [5]. One of the simplest classes of these electron-rich species consists of compounds with a tetrahedral cluster core of general formula M_2E_2 (M = transition metal and E = Bi or Te) in which the E–E edge of the tetrahedron is spanned either by a carbene or by an isolobal ML_n organometallic fragment [11]. In the analysis developed below, the bridging entity is not considered a vertex of the cluster [12*]. These compounds with structure labeled **A** in Scheme 1 are listed in Table 1, together with some of their structural parameters. The E–E distances suggest that a direct bonding interaction persists in these molecules.

All the compounds gathered in Table 1 are isoelectronic and have seven skeletal electron pairs (SEP) which may be used for bonding in the tetrahedral core, *i.e.* an excess of two electrons with respect to the effective atomic number (EAN) as well as to the PSEP formalisms. In fact, species with seven SEPs are expected to adopt a butterfly-type arrangement for their M_2E_2 core, such as **B** shown in Scheme 1, in which direct E–E bonding would not be expected. The lack of an E–E interaction is observed for isoelectronic and structurally similar edge-bridged clusters where E = S [13,14] or Se [14]. These compounds have the same geometry as **A** but the observed separation precludes direct E–E bonding. $[Fe_2(CO)_6(\mu\text{-}ER)_2]$ have the same electron count but are not constrained by a bridging group, and no direct E–E bond is proposed even for E = Te [15,16].

Correspondence to: Dr. J.-F. Halet or Professor J.-Y. Saillard.

* Reference number with asterisk indicates a note in the list of references.

0022-328X/94/$7.00
SSDI 0022-328X(93)E24130-W

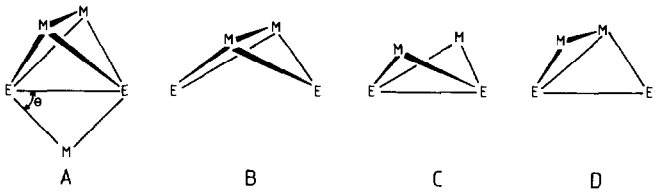

Scheme 1.

In the compounds listed in Table 1, the E ··· E separations are within the range of a standard single bond (for E = Bi) or slightly longer (*ca.* 15%) as for E = Te. The claw effect of the CR_2 or ML_n bridging units can be invoked to explain the fact that the two E atoms are within bonding distance. However, this is not observed when E = S or Se. Moreover, if there is a forced E–E contact, a strong destabilization should occur for the observed electron count, which could easily be relieved by opening, some other bond (M–M or M–E) of the tetrahedron, leading to alternative butterfly structures such as those presented in **C** and **D** of Scheme 1. Indeed, there are several examples of unbridged 7-SEP clusters adopting these structures [17,18].

The aim of this paper is to explain by means of extended Hückel calculations why the tetrahedral structure is nevertheless maintained in the complexes given in Table 1. The compound we have chosen to model is the bismuth species **1**, synthesized by one of us [6] and which should give rise to the strongest E–E interaction. Calculations on M_2Te_2 clusters give the same qualitative results. Computational details are given in the Appendix.

2. The tetrahedron $Fe_2(CO)_6Bi_2$

In order to understand the possible role played by the $Co(CO)_4$ bridging unit in **1**, we present first the electronic structure of the hypothetical unbridged tetrahedral $[Fe_2(CO)_6Bi_2]^{2-}$. Secondly, the interaction between the $[Fe_2(CO)_6Bi_2]^{2-}$ tetrahedron and the $Co(CO)_4$ bridging unit is considered. The molecular orbital (MO) diagram of $[Fe_2(CO)_6Bi_2]^{2-}$ is shown in Fig. 1, based on the interaction between the $Fe_2(CO)_6$ and Bi_2 fragments. Each $Fe(CO)_3$ fragment bears three frontier orbitals [11], giving rise to six frontier molecular orbitals (FMO) for the $[Bi_2Fe_2(CO)_6]^{2-}$ unit. These can be identified roughly as being the σ, σ^*, π and π^* levels associated with the Fe–Fe bond. The Bi_2 moiety exhibits the same types of σ, σ^*, π and π^* FMOs, with additional in-phase and out-of phase combinations of two lone pair orbitals on each Bi atom, which are expected to interact weakly with the metal fragment.

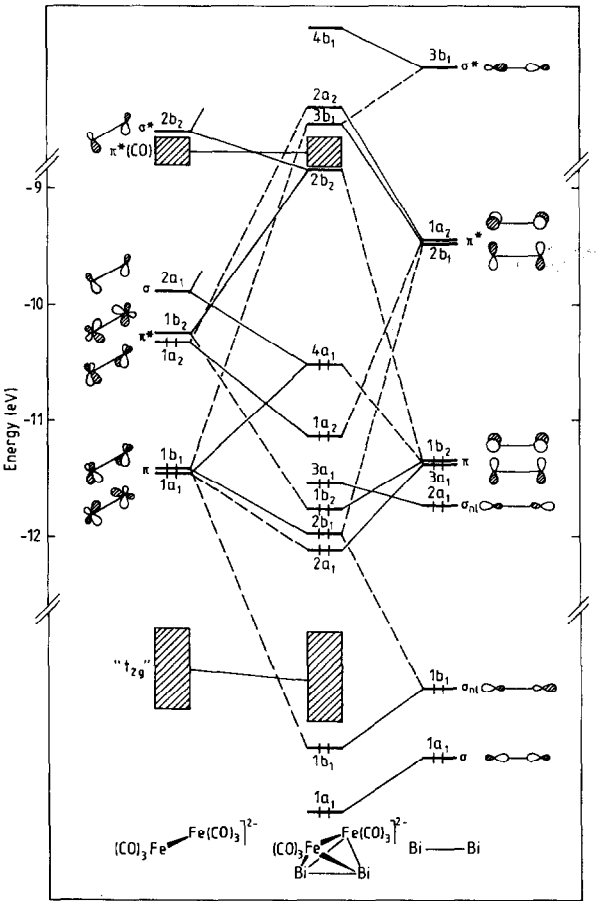

Fig. 1. Molecular orbital interaction diagram for the tetrahedral model $[Fe_2(CO)_6Bi_2]^{2-}$.

The resulting MO diagram of the $[Fe_2(CO)_6Bi_2]^{2-}$ unit is not discussed in detail here, since it is typical of

TABLE 1. Bridged mixed main-group/transition metal tetrahedral M_2E_2 clusters characterized by X-ray diffraction

Compound	SEP count	θ [a] angle (°) [b]	d(E ··· E) (Å)	Ref.
$[Fe_2(CO)_6(Bi_2)(\mu - Co(CO)_4)]^-$ (1)	7	57	3.092(2)	6
$[Fe_2(CO)_6(Te)_2(\mu - CH_2)]$ (2)	7	44	3.114(1)	7
$[Fe_2(CO)_6(Te)_2(\mu - Fe(CO)_4]$ (3)	7	54	3.111(1)	8
$[Fe_2(CO)_6(Te_2)(\mu - Fe(CO)_3PPh_3)]$ (4)	7	54	3.138(1)	9
$[FeMoCp(CO)_5(Te_2)(\mu - MoCp(CO)_2)]$ (5)	7	68	3.146(1)	10

[a] See text: [b] Averaged.

any tetrahedral framework resulting from the combination of four conical fragments, including tetrahedrane [5c,17,19]. In particular, it exhibits a large and unique energy gap (2.2 eV) between the $4a_1$ and $2b_2$ levels (see Fig. 1), strongly favouring the 6-SEP electron count, with the following formal skeletal configuration $(a_1)^6(a_2)^2(b_1)^2(b_2)^2$ [17]. In this way, the 6-SEP model $[Fe_2(CO)_6Bi_2]^{2-}$ is closely related to real tetrahedral species, such as $[Fe_2(CO)_6E_2]$ (E = S [20], Se [21], or Te [22]), $[Co_2(CO)_6As_2]$ [23], $[Co_2(CO)_5(PPh_3)As_2]$ [24], and $[Cp_2(CO)_4Mo_2As_2]$ [25]. Consistent with the 6-SEP favoured electron count, the computed overlap populations associated with the Bi–Bi, Fe–Bi and Fe–Fe bonds in $[Fe_2(CO)_6Bi_2]^{2-}$ are large (0.649, 0.358, and 0.172, respectively). The addition of an extra electron pair to the $2b_2$ LUMO leads to a negative Fe–Fe (−0.028) and a smaller Bi–Bi (0.315) overlap population, indicating that such a 7-SEP species would be more stable in one of the structures **C** or **D** rather than **A**, consistent with the EAN and PSEP rules.

We focus now on the cluster orbitals of symmetry b_1, which play a crucial role in the interaction of $[Fe_2(CO)_6Bi_2]^{2-}$ with the bridging unit (*vide supra*). In principle, for the count of 7 SEPs, there are formally four skeletal molecular orbitals (SMO) of b_1 symmetry (of which two are occupied and two unoccupied) and one b_1 level associated with the Bi lone pairs. However, mixing occurs between these SMOs and the lone pair orbital, as described below. The low-energy $1b_1$ level of the Fe_2Bi_2 tetrahedron derives primarily from the $1b_1$ out-of-phase combination of the lone pairs of the Bi_2 fragment, mixed in a bonding way with the $1b_1$ π-bonding FMO of the $Fe_2(CO)_6$ unit. The $2b_1$ level of the tetrahedron has an overall 54% localization on the Bi_2 fragment. The contribution of the $2b_1$ π-antibonding FMO of Bi_2 is 38%, while the contribution of the $1b_1$ lone-pair combination is 13%. These two Bi_2 levels mix with the $1b_1$ FMO of $Fe_2(CO)_6$ in such a way that the resulting $2b_1$ MO of the tetrahedron is bonding between the Bi_2 and $Fe_2(CO)_6$ fragments. This three-orbital mixing pattern is illustrated in Scheme 2(a). A plot of this $2b_1$ molecular orbital is given in Fig. 2(a). The lowest unoccupied cluster orbital of b_1 symmetry, namely $3b_1$, also has a substantial bismuth character (72%). The major Bi_2 FMO contributions come from $2b_1$ (46%) and $3b_1$ (23%). They also mix mainly with the $1b_1$ FMO of $Fe_2(CO)_6$, in such a way that the resulting cluster $3b_1$ level is antibonding. This three-orbital mixing pattern is shown in Scheme 2(b). The resultant MO is plotted in Fig. 2(b). Finally, the $4b_1$ cluster MO, situated at very high energy, derives largely from the $3b_1$ σ-antibonding FMO of the Bi_2 entity.

As discussed below, orbitals of a_1 and b_1 symmetry are able to interact with the bridging fragment. Thus,

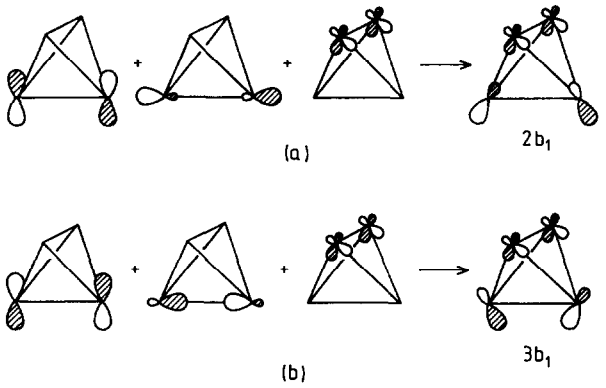

Scheme 2.

from the above discussion we can see that the two frontier orbitals of b_1 symmetry of the 6-SEP $[Fe_2(CO)_6Bi_2]^{2-}$ tetrahedral model with which we need be concerned are the $2b_1$ (highest occupied) and $3b_1$ (lowest unoccupied) levels. It is important to remember in the following discussion that the main lobes of the these two orbitals on the Bi_2 fragment are differently oriented (see Scheme 2 and Fig. 2).

3. The bridged tetrahedral molecule $[Fe_2(CO)_6Bi_2\{\mu\text{-}Co(CO)_4\}]^-$ (1)

The MO diagram of the 7-SEP anionic compound **1** is given in Fig. 3, based on the formal interaction of the

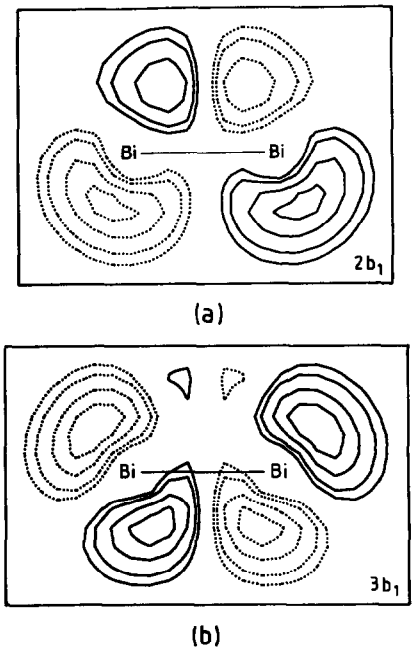

Fig. 2. Contour maps of the $2b_1$ (a) and $3b_1$ (b) FMOs of the tetrahedral $[Fe_2(CO)_6Bi_2]^{2-}$ species. Only the bismuth part is shown and plotted in the plane passing through the two Bi atoms and the middle of the Fe–Fe vector.

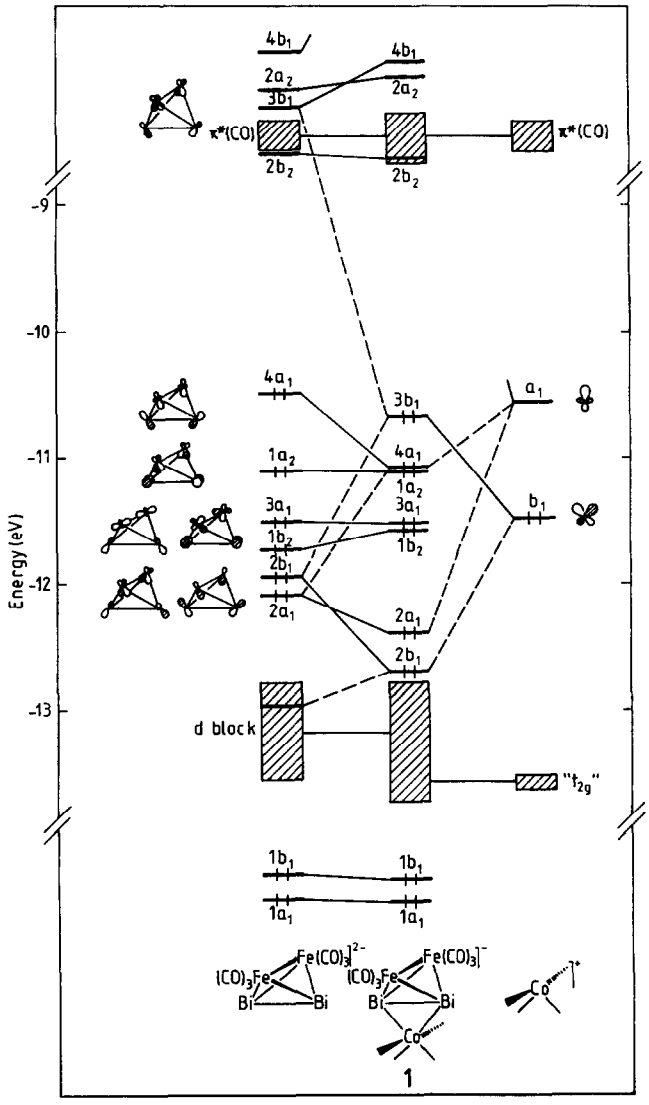

Fig. 3. Molecular orbital interaction diagram for the bridged tetrahedral molecule $[Fe_2(CO)_6Bi_2(\mu\text{-}Co(CO)_4)]^-$.

$[Fe_2(CO)_6Bi_2]^{2-}$ tetrahedron with the $[Co(CO)_4]^+$ bridging moiety. The latter C_{2v} ML_4 fragment possesses a set of two frontier orbitals, lying significantly above the so-called "t_{2g}" set [11]. One is a σ-type hybrid of a_1 symmetry, the other is a π-type hybrid of b_1 symmetry. Usually, the presence of a bridging unit on an edge of a cluster cage is not expected to change the favoured electron count. In other words, each of its frontier orbitals is expected to interact with the orbitals of the cluster in such a way that the resulting number of bonding and non-bonding orbitals is the same with and without the bridge [11c]. As stated previously, this is not the case for **1**, which bears two electrons more than the unbridged tetrahedral parent and consequently is in disagreement with the count expected from the PSEP rules. One can see in Fig. 3 that the calculations are entirely consistent with the observed stability of **1**. Indeed, a large HOMO/LUMO gap of 2.15 eV is computed for the actual 7-SEP count, while a HOMO/LUMO gap which is too small (0.44 eV) is found with the count of 6 SEPs.

According to Fig. 3, the a_1 FMO of the $[Co(CO)_4]^+$ fragment is strongly destabilized by the $2a_1$ and $4a_1$ levels of the unbridged tetrahedron, giving rise to a strongly antibonding and very high-lying combination. It follows that the number of occupied a_1 levels is the same in the bridged and unbridged clusters. In contrast, this is not the case for the number of b_1 levels. The b_1 FMO of the $[Co(CO)_4]^+$ unit interacts, in turn, principally with the $2b_1$ and $3b_1$ levels of the $[Fe_2(CO)_6Bi_2]^{2-}$ tetrahedron. Its interaction with the low-lying $2b_1$ gives rise to a destabilizing contribution, while its interaction with the high-lying $3b_1$ induces a stabilizing contribution. From an energy point of view, one might expect that the destabilizing contribution should largely dominate, since the $2b_1$ cluster level is closer in energy to the b_1 FMO of $[Co(CO)_4]^+$. This is not the case, as one can see in Fig. 3; this destabilization is largely counterbalanced by stabilization due to the interaction with the cluster $3b_1$ level. The reason lies in the overlap between the b_1 FMO of $[Co(CO)_4]^+$ with $3b_1$ (0.217) which is larger than that with $2b_1$ (0.148). It follows that the resulting $3b_1$ MO combination of the bridged species $[Fe_2(CO)_6Bi_2\{\mu\text{-}Co(CO)_4\}]^-$ stays at low energy, being more non-bonding in character than really antibonding. Therefore, it has to be populated to provide some stability to the cluster. Thus, the extra skeletal electron pair of **1** lies in the $3b_1$ MO, and the reason for this electron excess seems obvious when we look at Scheme 2 and Fig. 2. The main lobes of the $3b_1$ FMO of the unbridged cluster point towards the cobalt atom, leading to a strong overlap with the latter, while they are badly oriented in the $2b_1$ FMO. Clearly, the claw effect of the bridging ligand is one of the parameters which favours the electron excess in these species, by favouring the overlap with $3b_1$. This effect is analyzed in the next section.

The computed Bi–Bi, Fe–Bi, Fe–Fe and Co–Bi overlap populations in the 7-SEP compound **1** are 0.429, 0.373, 0.177, and 0.234, respectively, indicative of strong bonding. However, comparison of the Bi–Bi value with the corresponding one in the 6-SEP unbridged $[Fe_2(CO)_6Bi_2]^{2-}$ species indicates that the addition of the $[Co(CO)_4]^+$ bridge weakens the Bi–Bi bond significantly (0.649 *vs.* 0.429). This is mainly due to the occupation of the $3b_1$ level in **1**. Indeed, this level has significant participation (14%) of the vacant $3b_1$ FMO of $[Fe_2(CO)_6Bi_2]^{2-}$, which is strongly Bi–Bi antibonding (see Figs. 1–3). The interaction of a_1 symmetry also contributes to the weakening of the Bi–Bi

bond, since it produces a depopulation of the occupied $2a_1$ and $4a_1$ Bi–Bi bonding orbitals of the unbridged cluster (by 0.17 and 0.63 electrons, respectively).

4. Angular analysis of the claw effect

The claw effect of the $Co(CO)_4$ fragment in **1** can be evaluated by replacing this bridging unit by two terminal substituents (such as hydrogen atoms) on the bismuth atoms. Such a set of two terminal hydrogen atoms is isolobal to $Co(CO)_4$ [11] in that it also has a set of two (a_1 and b_1) frontier orbitals, namely the in-phase and out-of-phase combinations of the two hydrogen 1s atomic orbitals. The pinch effect can be analyzed on the resulting 6/7-SEP $[Fe_2(CO)_6(BiH)_2]^{0/2-}$ model by varying the angle θ as shown in Scheme 3. The corresponding Walsh diagram and total energy curves are shown in Fig. 4. The main feature of this Walsh diagram is the strong stabilization of a level of b_1 symmetry when θ varies from 150° to about 70°. Below $\theta = 70°$, its energy starts to increase strongly, because of H···H and Bi···H steric interactions. For the count of 7 SEPs, this $3b_1$ level is occupied, driving the total energy to be minimum around $\theta = 75°$. In that case, the electronic structure of $[Fe_2(CO)_6(BiH)_2]^{2-}$ is similar to that of **1**. For the count of 6 SEPs, the total energy curve shows a flat minimum around $\theta = 130°$. For this value of θ, the H–Bi vectors are pointing roughly towards the centroid of the tetrahedral core. This is the typical situation of the classical 6-SEP tetrahedral clusters of general formula $[M_2L_n(ER)_2]$, such as $[Fe_2(CO)_6(NMe)_2]$[26] and $[Fe_2(CO)_6(P^tBu)_2]$. [27].

The behaviour of the crucial b_1 level with variation of θ can be understood from Fig. 5, which represents the interaction between the frontier orbitals of b_1 symmetry of the $Fe_2(CO)_6$ and H···H fragments in the $[Fe_2(CO)_6(BiH)_2]^{0/2-}$ model. For large values of θ, the H···H b_1 orbital overlaps mainly with the low-lying $2b_1$ FMO of the Fe_2Bi_2 tetrahedron, whose main lobes are pointing towards the H atoms. Consequently, the H···H b_1 level is strongly destabilized and becomes too antibonding to be occupied, and the favoured electron count is 6 SEPs, as predicted by the PSEP rules. For small values of θ, the H···H b_1 orbital overlaps principally with the high-lying $3b_1$ FMO of the tetrahedron, whose main lobes are now pointing towards the H atoms. In this case, the strongly stabilizing interaction arising from the $3b_1$ FMO of the tetrahedron prevents the H···H b_1 orbital from being significantly raised in energy. Therefore, it remains more or less non-bonding and can be occupied, leading to the 7-SEP favoured electron count.

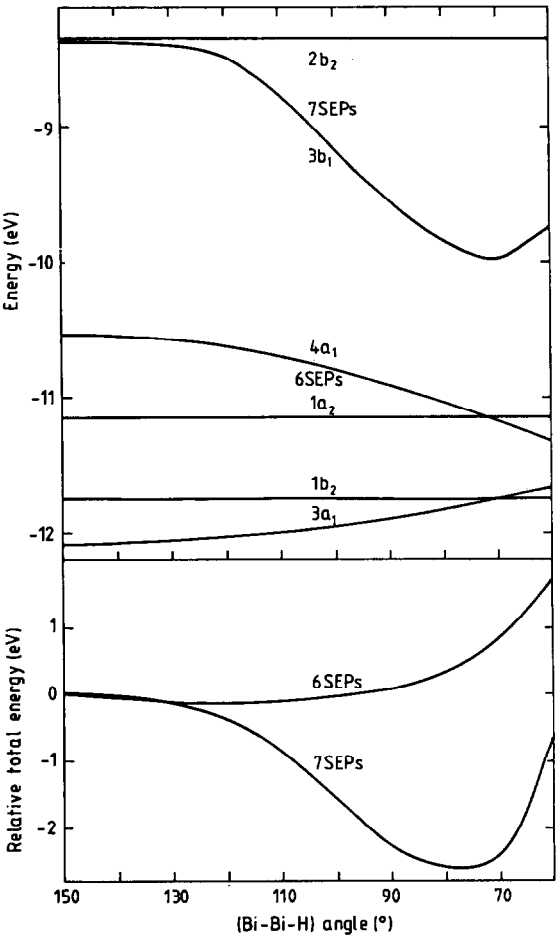

Fig. 4. Walsh diagram and total electronic energy variation as function of the (Bi–Bi–H) angle (θ) in the tetrahedral model $[Fe_2(CO)_6(BiH)_2]^{0/2-}$.

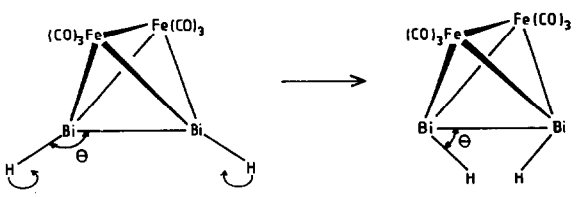

Scheme 3.

5. Related compounds

In compound **2** of Table 1, a carbene bridges the Te_2 linkage. As stated previously, a CR_2 fragment is isolobal to the $[Co(CO)_4]^+$ unit [11]. We checked their related electronic effects by substituting the $[Co(CO)_4]^+$ bridge in **1** by a methylene group, CH_2. Calculations on the resulting $[Fe_2(CO)_6Bi_2(\mu\text{-}CH_2)]^{2-}$ model lead to results qualitatively similar to that obtained for **1**. In particular, the calculated HOMO/LUMO gap is large (1.87 eV), and the computed

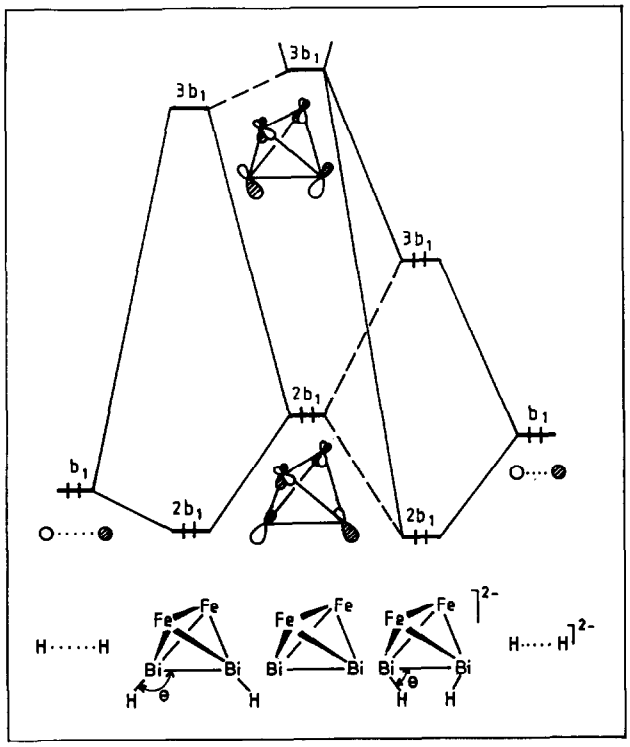

Fig. 5. Interaction diagram between the b_1 FMOs of the $Fe_2(CO)_6$ and H · · · H moieties in the tetrahedral model $[Fe_2(CO)_6(BiH)_2]^{0/2-}$ for $\theta = 150°$ (on the left) and $\theta = 70°$ (on the right).

Fe–Bi and Fe–Fe overlap populations (0.371 and 0.188, respectively) compare well with the corresponding values found for **1** (0.373 and 0.177, respectively). This is not the case for the Bi–Bi overlap population, which is significantly smaller in $[Fe_2(CO)_6Bi_2(\mu\text{-}CH_2)]^{2-}$ (0.195 *vs.* 0.429 in **1**). The weakening of the Bi–Bi bond compared to **1**, results primarily from a stronger interaction between the b_1 FMO of CH_2 and the $3b_1$ orbital of the unbridged tetrahedron, but also from a stronger bonding interaction between the frontier orbitals of a_1 symmetry.

At this point of the discussion, it should be noted that, in order to secure a significant HOMO/LUMO gap in the 7-SEP bridged tetrahedron, the bridging entity must have its b_1 FMO sufficiently low in energy. This is indeed the case for all the compounds listed in Table 1. For example, calculations on the hypothetical $[Fe_2(CO)_6Bi_2(\mu\text{-}CO)]$ model lead to a unique electron count of 6 SEPs, because of the high energy of its b_1 (π^*_{CO}) frontier orbital.

As noted previously, the Te–Te separations in the tellurium clusters in Table 1 are roughly 10–15% longer than usual Te–Te single bonds and therefore, slightly weaker than the Bi–Bi bond in compound **1**. Here there is a second parameter which plays an important role in the E–E bonding in the bridged mixed main-group/transition metal M_2E_2 species, electronegativity. Since Te is more electronegative than Bi, the $3b_1$ FMO of the unbridged tetrahedron, which is strongly E–E antibonding for the case of bismuth, has a lower energy in the case of Te. Consequently, it interacts more strongly with the bridge and its occupation will be more important after interaction, leading to a weaker E–E bond. With E = Se or S, this electronegativity effect is even larger, and the E · · · E bonding character is completely missing [13,14].

In the Introduction, we mentioned that the 7-SEP unbridged $[Fe_2(CO)_6(\mu\text{-}TeMe)_2]$ [15,16] adopts the butterfly structure **B**, in agreement with the EAN and PSEP rules. Although in this compound the Te · · · Te distance (3.26 Å) appears to lie out of the range of significant bonding contacts, one could argue that some weak bonding interaction could remain, despite the unbridged nature of the tetrahedron. The nature of this through-space interaction has been investigated on the idealized model $[Fe_2(CO)_6(TeH)_2]$. The electronic configuration is typical of any classical electron-precise butterfly cluster. The calculated HOMO/LUMO gap (2.4 eV) is large, consistent with the stability of $[Fe_2(CO)_6(\mu\text{-}TeMe)_2]$ [15]. The computed Te · · · Te overlap population is slightly positive (+0.033), indicating a weak bonding interaction. In the deprotonated isoelectronic $[Fe_2(CO)_6(Te)_2]^{2-}$ fragment, the Te · · · Te overlap population is slightly negative (−0.044), because of the occupation of the $3b_1$ FMO in this 7-SEP open tetrahedron. When the protons are added to the Te atoms, their b_1 FMO interacts principally with the $3b_1$ level of $[Fe_2(CO)_6(Te)_2]^{2-}$ which is higher in energy, due to the electropositive nature of tellurium. Consequently, the resulting antibonding vacant combination bears a large Te contribution. As a result, the somewhat Te · · · Te antibonding $3b_1$ FMO of $[Fe_2(CO)_6(Te)_2]^{2-}$ is partly depopulated under protonation, leading to a weak Te · · · Te attraction. This attraction is expected to disappear upon substitution of Te by a more electronegative element such as S [17,18], while it should increase upon substitution by a more electropositive element such as Bi^-.

The formation of a E · · · E interaction may be responsible for the experimental observation that donors add to $[Fe_3(CO)_9E_2]$ (E = Te) to give the bridged-tetrahedral structure **A**, whereas for E = S or Se, this does not happen.

6. Concluding remarks

To summarize, one can say that, because of the small pinch angle θ, the b_1 FMO of the $Co(CO)_4$ bridge is prevented from interacting strongly with the $2b_1$ orbital of the $Fe_2(CO)_6Bi_2$ fragment. This $2b_1$

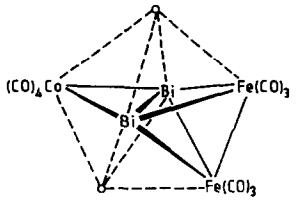

Scheme 4.

orbital can be roughly identified as the out-of-phase combination of the Bi lone pairs of the $Fe_2(CO)_6Bi_2$ tetrahedron. However, this b_1 FMO interacts preferentially with the $3b_1$ orbital of the $Fe_2(CO)_6Bi_2$ fragment, which is Bi–Bi π/σ-antibonding and therefore can be identified as being a skeletal MO. This suggests that the $Co(CO)_4$ fragment could be considered as being part of the cluster, and not simply as a bridging ligand. In that way, compound **1** can be viewed alternatively as an *arachno*-pentagonal bipyramidal cluster (i.e. with two unoccupied vertices) as shown in Scheme 4. For such an *arachno* species of M_3E_2 skeleton, PSEP theory predicts a count of 8 SEPs. Accordingly, compound **1** bears 8 SEPs with respect to the pentagonal bipyramid. Indeed, to the 7 SEPs associated with the Fe_2Bi_2 tetrahedron, one must add one "t_{2g}" nonbonding electron pair of b_2 symmetry deriving from the $Co(CO)_4$ unit, in order to render it isolobal with a conical fragment [11].

We have described previously the structure, and analyzed the bonding of, pentagonal bipyramidal *nido*-type clusters (*i.e.* with one vacant vertex) of the Co_4Bi_2 skeleton, shown in Scheme 5(a). In particular, we deduced the the "through-cluster" Bi–Bi bonding in these species is related to a size effect and to the electronegativity difference between Co and Bi [5c]. In fact, these compounds have 9 SEPs, while only 8 are expected from PSEP theory. Our calculations on the $[Co_4(CO)_{12}Bi_2]$ and $[Co_4(CO)_{10}(\mu\text{-}CO)Bi_2]^{2-}$ showed that the excess electron pair occupies a rather low-lying Co–Co π-antibonding level. The possibility of a 9-SEP count for a related arachno-type $[Co_3(CO)_9Bi_2]^-$ species shown in Scheme 5(b) then arises. Calculations on $[Co_3(CO)_9Bi_2]^-$, generated from $[Co_4(CO)_{12}Bi_2]$ by simply removing one $[Co(CO)_3]^+$ group, indicate that

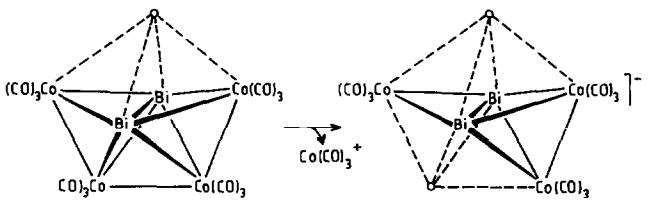

Scheme 5.

an 8-SEP count is the only possibility. Indeed, the low-lying Co-Co π-antibonding level present in the *nido* species disappears in $[Co_3(CO)_9Bi_2]^-$, due to the loss of Co–Co contacts. In fact, the electronic structure of this model is very similar to that of **1**.

The size and electronegativity effects have been invoked to explain the Bi–Bi bonding in the *nido* $[Co_4(CO)_{12}(\mu\text{-}CO)Bi_2]$ and related species [5c]. These parameters are also valid for the arachno species such as **1**, listed in Table 1. Indeed, the covalent radius of the main-group atom E has to be large enough to produce a pinch angle θ small enough to interact with the $3b_1$ FMO of the unbridged tetrahedral core. Moreover, E must be significantly more electropositive than M, so that the crucial $3b_1$ FMO of the unbridged tetrahedron, depicted in Fig. 2(b), has a preponderant localization on the E–E hinge, not on the M–M bond. The fact that E is electropositive also means that its atomic orbitals are diffuse, able to provide significant overlap in any direction. Clearly, the problem we are dealing with in this paper is, in some ways, related to hypervalency of main-group elements. From this point of view, it is interesting to note that the coordination sphere around each Bi atom in compound **1**, resembles that of sulfur in the typical hypervalent molecule SF_4 for instance [28,29].

Acknowledgment

We are grateful to L. Hubert for his expertise in the drawings.

References and notes

1 (a) K. Wade, *J. Chem. Soc., Chem. Commun.*, (1971) 792; (b) K. Wade, *Adv. Inorg. Chem. Radiochem.*, *18* (1976) 1; (c) K. Wade, in *Transition Metal Clusters*, B.F.G. Johnson (ed.), Wiley, New York, 1980, p. 193.

2 (a) D.M.P. Mingos, *Nature (London) Phys. Sci.*, *236* (1972) 99; (b) D.M.P. Mingos, *Acc. Chem. Res.*, *17* (1984) 311; (c) D.M.P. Mingos and R.L. Johnston, *Struct. Bond. (Berlin)*, *68* (1987) 29; (d) D.M.P. Mingos and D.J. Wales, *Introduction to Cluster Chemistry*, Prentice Hall, Englewood Cliffs, NJ, 1990.

3 B.K. Teo, *J. Chem. Soc., Chem. Commun.*, (1983) 1362, (b) B.K. Teo, *Inorg. Chem.*, *23* (1984) 1251, (c) B.K. Teo, G. Longoni and F.R. Chung, *Inorg. Chem.*, *23* (1984) 1257, (d) B.K. Teo, *Inorg. Chem.*, *24* (1985) 1627.

4 (a) R.B. King and D.H. Rouvray, *J. Am. Chem. Soc.*, *99* (1977) 7834; (b) R.B. King, *Inorg. Chim. Acta*, *116* (1986) 99, 119, 125.

5 See for example: (a) J.-F. Halet, R. Hoffmann and J.-Y. Saillard, *Inorg. Chem.*, *25* (1985) 1695; (b) J.-F. Halet and J.-Y. Saillard, *New J. Chem.*, *11* (1987) 315; (c) T.A. Albright, K. Ae Yee, J.-Y. Saillard, S. Kahlal, J.-F. Halet, J.S. Leigh and K.H. Whitmire, *Inorg. Chem.*, *30* (1991) 1179; (d) D.N. Cox, D.M.P. Mingos and R. Hoffmann, *J. Chem. Soc., Dalton Trans.*, (1981) 1178.

6 K.H. Whitmire, K.S. Raghuveer, M.R. Churchill, J.C. Fettinger and R.F. See, *J. Am. Chm. Soc.*, *108* (1986) 2778.

7 (a) P. Mathur and V.D. Reddy, *J. Organomet. Chem.*, *387* (1990)

193; (b) P. Mathur, V.D. Reddy and R. Bohra, *J. Organomet. Chem.*, *401* (1991) 339.
8 G. Gervasio, *J. Organomet. Chem.*, *441* (1992) 271.
9 D.A. Lesch and T.B. Rauchfuss, *Organometallics*, *1* (1982) 499.
10 L.E. Bogan, T.B. Rauchfuss and A.L. Rheingold, *J. Am. Chem. Soc.*, *107* (1985) 3843.
11 (a) M. Elian and R. Hoffmann, *Inorg. Chem.*, *14* (1974) 1058; (b) R. Hoffmann, *Angew. Chem., Int. Ed. Engl.*, *21* (1982) 711; (c) D.G. Evans and D.M.P. Mingos, *Organometallics*, *2* (1983) 435.
12 For metal-bridged clusters, a different electron count is obtained when the bridging metal is considered part of the cluster skeleton (see Section 6).
13 See for example: (a) D.A. Lesch and T.B. Rauchfuss, *J. Organomet. Chem.*, *199* (1980) C6; (b) G.I. Lilley, E. Sinn and B.A. Averill, *Inorg. Chem.*, *25* (1986) 1073.
14 V.W. Day, D.A. Lesch and T.B. Rauchfuss, *J. Am. Chem. Soc.*, *104* (1982) 1290.
15 R.E. Bachman and K.H. Whitmire, *Organometallics*, *12* (1993) 1988.
16 The similar anion $[Fe_2(CO)_6(Te)(Te_2)]^{2-}$ has been characterized: B.W. Eichhorn, R.C. Haushalter and J.S. Merola, *Inorg. Chem.*, *29* (1990) 728.
17 See for example: (a) J.-F. Halet and J.-Y. Saillard, *J. Organomet. Chem.*, *327* (1987) 365 and refs. therein, (b) M. El Khalifa, F.Y. Pétillon, J.-Y. Saillard and J. Talarmin, *Inorg. Chem.*, *28* (1989) 3849.
18 (a) D. Seyferth and R.S. Henderson, *J. Am. Chem. Soc.*, *101* (1979) 508; (b) D. Seyferth, R.S. Henderson and L.C. Song, *J. Organomet. Chem.*, *192* (1980) C1; (c) D. Seyferth, R.S. Henderson and L.C. Song, *Organometallics*, *1* (1982) 125; (d) J.R. Dilworth and S. Morton, *J. Organomet. Chem.*, *314* (1986) C25; (e) R.D. Weatherhill, T.B. Rauchfuss and R.A. Scott, *Inorg. Chem.*, *25* (1986) 1466; (f) R.L. De Kock, E.J. Baerends and R. Hengelmolen, *Organometallics*, *3* (1984) 289; (g) J.A. Kovacs, J.K. Bashkin and R.H. Holm, *Polyhedron*, *6* (1987) 1445.
19 D.M. Hoffman, R. Hoffmann and C.R. Fisel, *J. Am. Chem. Soc.*, *104* (1982) 3858.
20 L.F. Dahl and C.H. Wei, *Inorg. Chem.*, *4* (1965) 493.
21 C.F. Campana, F.Y.-K. Lo and L.F. Dahl, *Inorg. Chem.*, *18* (1979) 3060.
22 D.A. Lesch and T.B. Rauchfuss, *Inorg. Chem.*, *20* (1981) 3583.
23 A.S. Foust, M.S. Foster and L.F. Dahl, *J. Am. Chem. Soc.*, *91* (1969) 5633.
24 S.A. Foust, C.F. Campana, D. Sinclair and L.F. Dahl, *Inorg. Chem.*, *18* (1979) 3047.
25 P.J. Sullivan and A.L. Rheingold, *Organometallics*, *1* (1982) 1547.
26 R.J. Doedens and J.A. Ibers, *Inorg. Chem.*, *8* (1969) 2709.
27 H. Vahrenkamp and D. Wolters, *Angew. Chem., Int. Ed. Engl.*, *22* (1983) 154.
28 K. Kimura and S.H. Bauer, *J. Chem. Phys.*, *39* (1963) 3172.
29 T.A. Albright, J.K. Burdett and M.-H. Whangbo, *Orbital Interactions in Chemistry*, Wiley, New York, 1985.
30 (a) R. Hoffmann, *J. Chem. Phys.*, *39* (1963) 1397; (b) R. Hoffmann and W.N. Lipscomb, *J. Chem. Phys.*, *36* (1962) 2179, 3489; *37* (1962) 2872.
31 J.H. Ammeter, H.-B. Bürgi, J.C. Thibeault and R. Hoffmann, *J. Am. Chem. Soc.*, *100* (1978) 3686.

Appendix

All computations were carried out within the extended Hückel method [30] with use of the modified Wolfsberg–Helmholz formula [31]. The atomic parameters utilized are given in Table 2. Structural parameters for the different models were taken from the idealized crystallographic data of compound **1**. In the $[Fe_2(CO)_6Bi_2(\mu\text{-}CH_2)]^{2-}$ model, the Bi–C(H_2) and C–H separations were set equal to 2.68 Å and 1.09 Å, respectively. The Bi–H distance of 1.8 Å was used in the models $[Fe_2(CO)_6(BiH)_2]^{0/2-}$. The experimental structure of $[Fe_2(CO)_6(TeMe)_2]$ was idealized and used for the model $[Fe_2(CO)_6(TeH)_2]$ [15]. A Te–H distance of 1.65 Å was used. The geometry of the model $[Co_3(CO)_9Bi_2]^-$ was obtained from the idealized experimental structure of $[Co_4(CO)_{10}(\mu\text{-}CO)Bi_2]^{2-}$ by removal of a $Co(CO)_3$ fragment [5c].

TABLE 2. Extended Hückel parameters

Orbital		H_{ii} (eV)	ζ_1	ζ_2	c_1 [a]	c_2 [a]
H	1s	−13.60	1.300			
C	2s	−21.40	1.625			
	2p	−11.40	1.625			
O	2s	−32.30	2.275			
	2p	−14.80	2.275			
Te	5s	−20.80	2.510			
	5p	−13.2	2.160			
Bi	6s	−15.75	2.653			
	6p	−10.52	2.092			
Fe	4s	−9.10	1.900			
	4p	−5.32	1.900			
	3d	−12.60	5.350	1.80	0.5366	0.6678
Co	4s	−9.21	2.000			
	4p	−5.29	2.000			
	3d	−13.18	5.550	1.90	0.5551	0.6461

[a] Coefficients in the double-ζ expansion.